DNA METHYLTRANSFERASE 3 (MET3) is regulated by Polycomb Group complex during Arabidopsis endosperm development

Louis Tirot[1] and Pauline E. Jullien[1†]

[1] Institute of Plant Sciences, University of Bern, Bern, Switzerland.

[†]*Corresponding author:* Pauline E. Jullien (pauline.jullien@ips.unibe.ch)

Key message

The DNA METHYLTRANSFERASE MET3 is controlled by Polycomb group complex during endosperm development.

Abstract

Complex epigenetic changes occur during plant reproduction. These regulations ensure the proper transmission of epigenetic information as well as allowing for zygotic totipotency. In *Arabidopsis*, the main DNA methyltransferase is called MET1 and is responsible for methylating cytosine in the CG context. The *Arabidopsis* genome encodes for three additional reproduction-specific homologs of *MET1*, namely *MET2a*, *MET2b* and *MET3.* In this paper, we show that the DNA methyltransferase *MET3* is expressed in the seed endosperm and its expression is further restricted to the chalazal endosperm. *MET3* is biallelically expressed in the endosperm but displays a paternal expression bias. We found that *MET3* expression is regulated by the Polycomb complex proteins FIE and MSI1. Seed development is not impaired in *met3* mutant, and we could not observe significant transcriptional changes in *met3* mutant. Interestingly, we found that *MET3* regulates gene expression in a Polycomb mutant background suggesting a further complexification of the interplay between H3K27me3 and DNA methylation in the seed endosperm.

Keywords

DNA methylation, *Arabidopsis*, endosperm, Polycomb, *MET3*

26 *Introduction*

27 Sexual reproduction in Angiosperm is initiated by a double fertilization event. Fertilization of the
28 haploid egg cell by one of the sperm cells gives rise to the diploid embryo whereas fertilization of the
29 homodiploid central cell gives rise to the triploid endosperm (Berger 2003; Costa et al. 2004). The
30 endosperm represents a nourishing tissue supporting embryo growth and is therefore key for proper
31 seed development. Cell divisions in the endosperm are initiated very rapidly following fertilization.
32 These divisions are initially occurring without cellularization and form a syncytium that will later
33 cellularize (Brown et al. 1999, 2003; Boisnard-Lorig et al. 2001). An additional peculiarity of the
34 endosperm, beyond its triploid syncytial nature, is being the seat of interesting epigenetic phenomena
35 and complex epigenetic regulation.

36 Endosperm development and cellularization are indeed regulated by the FIS Polycomb group
37 complex known to mediate Histone H3 Lysine 27 tri-methylation, a key silencing epigenetic mark.
38 Some of the key members of the FIS Polycomb group complex (FIS-PcG) are MEA, FIS2, FIE, and MSI1
39 (Chaudhury et al. 1997; Luo et al. 1999; Kiyosue et al. 1999; Yadegari et al. 2000; Köhler et al. 2003;
40 Guitton et al. 2004). In mutants affecting those genes, the endosperm fails to cellularize, resulting in
41 an arrest of embryo development and eventually seed abortion. Additionally, several genes were
42 found to be imprinted, *i.e.* only one parental allele is expressed whereas the other is epigenetically
43 silent, in the endosperm. This is the case, for example, of genes such as *FIS2*, *FWA*, *MEA* or *PHE1*
44 (Kinoshita et al. 1999, 2004; Luo et al. 2000; Köhler et al. 2005; Jullien et al. 2006). The silencing of
45 those endosperm imprinted genes relies principally on two epigenetic mechanisms: either regulation
46 by the FIS-PcG itself like for *MEA* or *PHE1* or silencing by DNA methylation like for *FWA* and *FIS2* (Jullien
47 and Berger 2009; Gehring 2013; Batista and Köhler 2020). Another epigenetic singularity of the
48 endosperm is of being relatively hypomethylated compared to other plant tissues (Gehring et al. 2009;
49 Hsieh et al. 2009). This hypomethylation is due in part to the activity of a DNA glycosylase called
50 DEMETER (Choi et al. 2002; Gehring et al. 2006; Hsieh et al. 2009) and likely also to the low expression
51 of canonical actors of the DNA methylation pathway (Jullien et al. 2012).

52 DNA methylation is a key epigenetic mark regulating gene expression and protecting genome
53 integrity by repressing transposons. In plant genomes, DNA methylation is found in three cytosine
54 contexts: CG, CHG and CHH (where H is any base except C). Methylation on these different contexts
55 relies on specific DNA methyltransferases. DNA methylation on CG sites relies on maintenance DNA
56 METHYLTRANSFERASE (MET) where the main ubiquitous enzyme is MET1. DNA methylation on CHG
57 sites relies on CHROMOMETHYLASE3 (CMT3) and an interplay with histone methylation (Lindroth et
58 al. 2001). DNA methylation on CHH site, due to its non-symmetrical nature, relies on the constant *de*
59 *novo* methylation pathway involving small RNA molecules as well as DOMAIN REARANGED
60 METHYLTRANSFERASE2 (DRM2) (Cao and Jacobsen 2002). In centromeric sequences, CHH
61 methylation also relies on CHROMOMETHYLASE2 (CMT2) (Stroud et al. 2013).

62 Although we know a lot about the main actors of this pathway, the *Arabidopsis*'s genome encodes
63 multiple copies of DNA methyltransferase genes (4 *METs*, 3 *CMTs* and 3 *DRMs*) some of which might
64 have a more complex or similar function in discreet cell types. For example, *CMT1* (the third
65 CHROMOMETHYLASE encoded by the *Arabidopsis* genome) is principally detected in reproductive
66 tissue (Henikoff and Comai 1998; Klepikova et al. 2016) and the reconstitution of a full-length
67 transcript relies on the splicing out of a transposable element situated in its 13th exon (Yadav et al.
68 2018). The *DOMAIN REARANGED METHYLTRANSFERASE1* (*DRM1*) seems to also solely play a role in
69 reproductive tissue, where a redundancy between *DRM1* and *DRM2* was observed in the early embryo
70 (Jullien et al. 2012). Similarly, data concerning the potential function of non-canonical *METs* are scarce.
71 *MET2a* and *MET2b* are detected in the central cell, but their function is unknown (Jullien et al. 2012).
72 Nonetheless, correlative evidence suggest *MET2a* might be important to regulate transposon
73 reactivation in wild *Arabidopsis* accessions (Quadrana et al. 2016) and involved in fungal response
74 (Salvador-Guirao et al. 2018).

75 As mentioned, little is known about the DNA methyltransferase *MET3*. *MET3* is also named
76 *MATERNAL EFFECT EMBRYO ARREST 57* (*MEE57*) as a transposon insertion associated with the *MET3*

77 locus led to an arrest in endosperm development (Pagnussat et al. 2005). *MET3* is also reported to be
78 the sole *MET* expressed in the endosperm (Jullien et al. 2012). Here, we show that *MET3* is specifically
79 expressed in the endosperm in a biallelic fashion with a paternal bias. *MET3* expression is controlled
80 by the FIS-PcG complex. Despite the initial report of a seed arrest phenotype in the *mee57* line, we
81 did not see any seed developmental phenotype in two independent *met3* mutant alleles. Additionally,
82 we could not see major changes in the seed transcriptome of *met3* mutant. Nevertheless, we could
83 see an effect on the seed transcriptome in a *fie* mutant background suggesting that *MET3* might
84 interplay with PcG gene regulation in the developing endosperm.

85 *Material and Methods*

86 *Plant Materials, Growth Conditions and Genotyping.*

87 The wild-types Col-0 and Gr-1, the *MET3* mutant lines *met3-3* (GABI404F04), *met3-4* (GABI659H03)
88 and PRC2 mutant lines *fie-362* (GABI_362D08) (Bouyer et al. 2011) and *msi1* (SAIL_429_B08) were
89 provided by the Nottingham Arabidopsis Stock Center (NASC). *pMET3:H2B-RFP* line was previously
90 described (Jullien et al. 2012). After sowing, plants were stratified in the dark at 4°C between 2 and 4
91 days. Plants were germinated and grown in growing chambers under long-day conditions (16h light
92 22°C / 8h dark 18°C). For the transmission analysis (Fig. S5b) , plants were grown on Murashige and
93 Skoog (MS1/2) media agarose plate in long-day conditions for 12 days before genotyping. Primers for
94 genotyping are listed in Table S1.

95 *Microscopy and phenotype observation*

96 DIC seed phenotype and GUS observations were done using a Leica DM2000 as previously described
97 (Jullien et al. 2006). For seed development observation and counting (Fig. 4a) , plants were
98 synchronized by removing all open flowers from the inflorescences. After 6 days, the two first siliques
99 situated above the previously removed flowers were picked for each inflorescence. We refer to this
100 stage as 6 days after synchronization (6 DAS). Siliques were dissected, cleared using chloride hydrate

101 solution and mounted on a slide for observation. *pMET3:H2B-tdTomato* and *pMET3:H2B-RFP* reporter
102 lines were imaged using a laser scanning confocal microscope (Leica SP5). When necessary, brightness
103 and contrast were uniformly modified by using ImageJ.

104 *Cloning and transformation*

105 *pMET3:H2B-tdTomato* and *pMET3:H2B-GUS* were generated using the Gateway Cloning System
106 (Invitrogen). All PCR fragments were amplified by PCR using the Phusion High-Fidelity DNA Polymerase
107 (Thermo). Primer sequences used for cloning can be found in Table S1. All plasmids were transformed
108 into wild-type Columbia-0 plants the by floral dipping method (Clough and Bent 1998). At least ten
109 transgenic lines were analyzed per construct, which showed a consistent fluorescence expression
110 pattern. An Illustration of the constructs can be found in Fig. S2a.

111 *RNA extraction, qPCR & RT-PCR*

112 Total RNAs were extracted using RNeasy Plant Minikit (Qiagen). All samples were treated with DNase
113 I (ThermoScientific) at 37°C for 30 minutes. DNAse I was subsequently inactivated by the addition of
114 EDTA and heat treatment (65°C for 10 minutes). First-strand cDNAs were synthesized using between
115 500 and 1000 ng of DNase treated total RNAs as a template. The RT reaction was performed using
116 either Maxima First Strand cDNA Synthesis Kit (Fig. 1a, Fig. 2a) (ThermoScientific) , containing both
117 oligo-dT and random hexamer primers, or RevertAid RT Reverse Transcription Kit (Fig. 3e, Fig. S4b)
118 (ThermoScientific) , containing only oligo-dT primers. The qPCR reactions were performed with a
119 QuantStudio 5 thermocycler (ThermoScientific) using SYBR green (KAPA SYBR FAST qPCR Master Mix
120 or ORA qPCR Green ROX H Mix). The qPCR mix was prepared according to the manufacturer's protocol.
121 An RNA equivalent of 25 ng of cDNA templates was used for each reaction. The qPCR program was as
122 follow: 95 °C for 3 minutes followed by 45 cycles of 95 °C for 5 seconds and 60 °C for 30 seconds.
123 *ACTIN2* (*AT3G18780*) expression was used to normalize the transcript level in each sample. For each
124 condition, RNA abundance of target genes was calculated from the average of three independent
125 biological replicates with three qPCR technical replicates. Real-time PCR primers used in this study are

126 listed in Table S1. For the allele-specific RT-PCR (Fig.2a) , cDNAs were amplified for 22 cycles for *ACT2*
127 primers and 35 cycles for *MET3* specific primers. Half of the *MET3* PCR product was digested for 1h30
128 at 37°C with XbaI restriction enzyme (Sigma-Aldrich). *ACT2* amplification was used as a control.

129 *RNA sequencing and Bioinformatics*

130 Total RNAs were extracted and DNAseI treated as previously mentioned. mRNA libraries were
131 prepared and sequenced by Novogene (https://en.novogene.com/). Bioinformatic analyses were
132 performed on the Galaxy web platform (https://usegalaxy.org) (Afgan et al. 2018). Our Galaxy
133 workflow including the exact parameters and tool versions used can be downloaded on
134 https://usegalaxy.org/u/pej/w/pejrnaseq and be freely reused. Briefly, Paired-end raw mRNA
135 sequencing reads were controlled using FastQC (Galaxy version 0.72) and trimmed using Trimmomatic
136 (Galaxy version 0.36.6) (Andrews 2010; Bolger et al. 2014). Clean reads were aligned to the *Arabidopsis*
137 *thaliana* TAIR 10 genome assembly using HISAT2 (Galaxy version 2.1.0+galaxy4) (Kim et al. 2015).
138 Aligned sequencing reads were assigned to genomic features using featureCounts (Galaxy version
139 1.6.2) (Liao et al. 2014). Differential expression was analyzed using DESeq2 default parameters (Galaxy
140 Version 2.11.40.6+galaxy1) (Love et al. 2014). Differentially expressed genes (DEGs) were defined by
141 an absolute logFC > 2 and an FDR < 0.05. Gene ontology (GO) enrichment analysis has been performed
142 on PANTHER (Mi et al. 2019) and visualized using REVIGO (Supek et al. 2011). All plots have been
143 generated using R-studio (www.rstudio.com). Raw data are deposited on GEO under reference XXXX.

144 *Results*

145 *MET3 is expressed biallelically with a paternal bias in the endosperm*

146 Our previous analysis has shown that *MET3* is expressed in the endosperm of developing
147 *Arabidopsis* seeds (Jullien et al. 2012). However, the detail and exclusivity of its expression pattern
148 remain to be investigated. To get a better characterization of *MET3* expression pattern, we performed
149 a qPCR of *MET3* transcript in different tissue types of wild-type Col-0 (Fig. 1a). Our result shows that

150 *MET3* is principally expressed in siliques and its expression peaks at 5 Days After Pollination (DAP).
151 These results could be confirmed using publicly available transcriptome datasets (Fig. S1a) (Klepikova
152 et al. 2016). To gain a better spatial and temporal characterization of *MET3* expression, we generated
153 two new transcriptional *MET3* reporter constructs, encompassing 2kb of the *MET3* promoter driving
154 either H2B-tdTomato or H2B-GUS (Fig. S2a). The analysis of the *pMET3:H2B-GUS* in different plant
155 tissues confirmed the specificity of *MET3* expression to the seed endosperm (Fig. S1b-d). To
156 characterize in detail the temporal expression of *MET3* in the endosperm, we performed confocal
157 microscopy on the *pMET3:H2B-tdTomato* lines at different stages of seed development. We could
158 detect *pMET3:H2B-tdTomato* expression from as early as the four nuclei stage endosperm (Fig. 1b).
159 *pMET3:H2B-tdTomato* remains express throughout the endosperm (Fig. 1c) until the globular stage of
160 embryo development where its expression starts to be higher in the chalazal endosperm and chalazal
161 cyst (Fig. 1d). At later stages, *pMET3:H2B-tdTomato* expression is limited to the chalazal endosperm
162 and chalazal cyst (Fig. 1e). From 7 DAP, *pMET3:H2B-tdTomato* expression can no longer be detected.
163 A similar expression pattern was observed with *pMET3:H2B-GUS* (Fig. S2b) and *pMET3:H2B-RFP* (Fig.
164 S2c) as well as online transcriptomic data (Fig. S2d) (Belmonte et al. 2013). MET3 protein expression
165 and localization could not be determined as we, so far, failed in expressing a fluorescently tagged
166 MET3 protein in *Arabidopsis* (LT personal communication).

167 Such endosperm expression pattern is common in imprinted genes, like *FWA*, *FIS2*, *MEA* or *PHE1*
168 (Kinoshita et al. 1999, 2004; Köhler et al. 2005; Jullien et al. 2006). In order to examine if *MET3* is
169 biallelically or mono-allelically expressed, we performed allele-specific RT-PCR. We are making use of
170 a Short Nucleotide Polymorphism (SNP) consisting of a substitution from a C to a T within *MET3* 9th
171 exon in the Gr-1 ecotype which is abolishing a XbaI restriction site present in Col-0. We did reciprocal
172 crosses using Col-0 and Gr-1 ecotypes and analyzed *MET3* parental expression at 5 DAP following XbaI
173 digestion (Fig. 2a). We could observe, for both reciprocal crosses, bands corresponding to *MET3*
174 transcript from Col-0 (505 and 329 bp) and from Gr-1 (834 bp) with a bias toward the paternal allele.
175 This result shows that *MET3* is expressed from both maternal and paternal allele but displays a

176 paternal bias of expression. *MET3* paternally biased expression was also observed using the
177 *pMET3:H2B-RFP* transgene at 1 DAP (Fig.2b). Taking together our results shows that *MET3* expression
178 is biallelic with a paternal bias and confined to the endosperm. *MET3* expression, initially throughout
179 the endosperm, becomes restricted to the chalazal pole at later stages.

180 *MET3 expression is regulated by Polycomb group proteins*

181 Beyond imprinted genes, *MET3* expression pattern is reminiscent of the expression of genes
182 controlled by the endosperm FIS Polycomb group complex (PcG) composed of FIE, MSI1, FIS2 and MEA
183 (Guitton et al. 2004). To investigate if *MET3* could be regulated by PcG, we introgressed a *MET3*
184 transcriptional reporter into *fie* and *msi1* mutant background (Fig. 3a-d). We could observe increased
185 *pMET3:H2B-RFP* reporter expression in 49% of the seeds (n=249) in *fie/+* mutant and 44% (n=240) in
186 *msi1/+* mutant background characteristic of the maternal gametophytic effect of those mutations (Fig.
187 3d). In *msi1* and *fie* mutants, *pMET3:H2B-RFP* expression is higher and observed throughout the
188 endosperm (Fig. 3b-c) whereas at the same developmental stage the expression of *pMET3:H2B-RFP* is
189 already restricted to the chalazal pole in wild-type seeds (Fig. 3a). In order to confirm that the
190 regulation of *MET3* by *MSI1* and *FIE* was not only restricted to our transgene, we performed a RT-qPCR
191 of *MET3* expression in wild-type and mutant selected seeds at 10 DAP (Fig. 3e). We could observe a
192 clear upregulation of *MET3* expression in both *fie* and *msi1* seeds compare to wild-type seeds (t-test
193 p-value of 0.0543 and 0.0114 respectively). Using publicly available data, we could see that the
194 upregulation of *MET3* is also observed in other PcG mutants (Fig. S3a-b). *MET3* upregulation was
195 observed in silique samples of *clf* mutant (Fig. S3a) (Liu et al. 2016) and in *fis2* seeds (Fig. S3b)
196 (Weinhofer et al. 2010).

197 Subsequently, we wanted to know if the effect of the PcG complex was direct or indirect. PcG
198 complexes are known to repress gene expression by tri-methylating the Lysine 27 of the Histone H3
199 tail (H3K27me3) inducing a closed chromatin state at the targeted loci. We, therefore, analyzed
200 available H3K27me3 genome-wide Chromatin Immunoprecipitation (ChIP) data. We could see that

201 the *MET3* locus is covered by H3K27me3 in *Arabidopsis* seedling samples (Fig. 3f) (Zhang et al. 2007).
202 Additionally, using the RepMap2020 tool (Chèneby et al. 2020) , we could observe H3K27me3 on the
203 *MET3* locus in several independent ChIP experiments including some performed on endosperm tissue
204 (Fig. S3c). We conclude that *MET3* expression is directly repressed by PcG complex induced H3K27me3
205 in the endosperm.

206 *MET3 does not affect seed development*

207 Considering that *MET3* is specifically expressed in the developing endosperm during seed
208 development, we then ask if *MET3* function influences seed and/or endosperm development. We
209 characterized two mutant alleles from the GABI collection: *met3-3* (GABI_404F04) and *met3-4*
210 (GABI_659H03) (Fig. S4a). The mutations are located on the 10th and the 2nd exon respectively and are
211 expected to abolish *MET3* function. To confirm the downregulation of *MET3* in the mutants, we
212 performed RT-qPCR. We could observe that *MET3* is downregulated in both mutant alleles (Fig. S4b).
213 To investigate if the *met3* mutation could result in seed lethality we first investigated the presence of
214 aborted seeds at the green seed stage (~12DAP). We could not see any significant seed abortion in
215 both *met3-3* and *met3-4* alleles (Fig. S5a). To further confirm the absence of defects, we analyzed the
216 transmission rate of the *met3* mutations in *met3-3/+* and *met3-4/+* selfed progeny. We could not
217 observe any segregation distortion from the Mendelian ratio (Fig. S5b). Mutations affecting the main
218 *Arabidopsis* DNA methyltransferase *MET1* display variation in seed size. We, therefore, investigated if
219 *met3* mutants would display a seed size phenotype. We could not see any significant variation in seed
220 size using both *met3* alleles (Fig. S5c-d). We conclude that *MET3* mutation does not severely impair
221 seed development.

222 As shown above, *MET3* expression is regulated by PcG complex in the endosperm, we then
223 analyzed if *MET3* mutation could influence the PcG *fie* mutant phenotype. To answer this question,
224 we generated *fie*/+;*met3-3* and *fie*/+;*met3-4* double mutants and analyzed their seed development
225 phenotype using DIC (Fig. 4a-f). In order to minimize the stress to the plant due to handling during

226 emasculation and crossing, we used “synchronized seeds”. In practice, we remove the open flowers
227 of the day, and we wait an x number of days before collecting two siliques above our cutting. This is
228 allowing us to have age synchronized siliques without the physical disturbance of
229 emasculation/pollination and is, therefore, closer to normal growth and fertilization. We are using the
230 term Day After Synchronization (DAS). To our experience, 6 DAS is corresponding to around 4-5DAP.
231 At 6 DAS, we could not see any delay in embryo development and endosperm cellularization
232 comparing Col-0 to *met3-3* and *met3-4* mutants (Fig. 4a-c, 4g-h). In *fie*/+, we could clearly see the
233 delayed endosperm cellularization characteristic of FIS-PcG mutants (Fig. 4d-f and h) (56% n=407)
234 (Ohad et al. 1999; Sørensen et al. 2001). In the double mutants, we could not see variations in the
235 quantification of the *fie*/+ phenotype for both embryo development (Fig. 4g) and endosperm
236 cellularization (Fig. 4h). We conclude that *MET3* mutations do not influence *fie* mutant seed
237 phenotype.

238 *Effect of MET3 mutation on the seed transcriptome*

239 In order to investigate the potential effect of *met3* mutation on the seed transcriptome, we
240 performed a mRNA deep sequencing experiment of 3 DAP (Fig. S6) and 10 DAS (Fig. 5a) seeds (*i.e.*
241 seeds attached to the septum). We then compared the seed transcriptome of *met3* seeds to wild-type
242 seeds. At 3 DAP, we could only detect one differentially expressed gene: *ESM1* (*AT3G14210*). *ESM1*
243 was up-regulated in both *met3-3* and *met3-4* mutant seeds (Fig. S6a-b). At 10 DAS, we could also only
244 see very minor changes to the seed transcriptome (Fig. 5a). We could identify only 16 differentially
245 expressed genes with an absolute logFC>2 and FDR<0.05. These results show that reminiscent of the
246 absence of seed phenotype in *met3* mutants, the seed transcriptome is also mostly unaffected by the
247 *met3* mutation. As *MET3* expression is regulated by the FIS-PcG complex in the endosperm, we then
248 ask if *MET3* mutation could influence the *fie* transcriptome. We, therefore, sequenced the
249 transcriptome of 10 DAS seeds where we selected for *fie* mutant seeds under the dissecting
250 microscope (white seeds). We compared the transcriptome of *fie* seeds to the transcriptome of
251 *fie;met3-3* double mutant seeds. We could observe 87 differentially expressed genes (DEG) with an

252 absolute logFC>2 and FDR<0.05 (Fig 5b). A Goterm enrichment analysis revealed that these genes are
253 enriched for genes involved in pectin metabolism (GO:0045490, FDR=4.46E-10; GO:0045488,
254 FDR=6.59E-09) and cell-wall related processes (GO:0042545, FDR= 8.97E-09; GO:0071555, FDR=4.87E-
255 10, GO:0071554, FDR=5.67E-08) (Fig. 5c and Table S2). We then analyzed if among these 87 DEGs
256 some are also modified in *fie* mutant compared to wild-type. We could find that a large proportion of
257 either *met3* DEGs (Col vs *met3*, 11/16) and *met3;fie* DEGs (*fie* versus *met3fie*, 44/87) are miss-
258 regulated in *fie* mutant seeds (Fig. 5d). We conclude that the *met3* mutation does not drastically
259 change the seed transcriptome, but a set of genes are miss-regulated by both *met3 and fie mutants*.

260 ## *Discussion*

261 Our study highlights an additional connection between DNA Methylation pathways and Polycomb
262 group H3K27 tri-methylation in the seed endosperm via the regulation of *MET3* by the FIS-PcG
263 complex. *MET3* is specifically expressed in the endosperm, and its expression becomes restricted to
264 the chalazal pole at later stages of endosperm development. In our study, using two independent
265 insertion lines, *met3-3* and *met3-4*, we could not observe any major seed developmental phenotype.
266 Both mutants show a significant decrease in *MET3* expression by qPCR suggesting they both represent
267 knockout mutants. It was previously documented that a mutation affecting *MET3* named *mee57*
268 displayed a strong seed developmental phenotype (Pagnussat et al. 2005). The *mee57* mutation shows
269 an early maternal embryo and endosperm arrest. The discrepancy between our lines and the
270 previously published *mee57* could have several causes: the mutagenesis method used (T-DNA versus
271 transposition) , the presence of additional genetic modifications, or a difference between the two
272 ecotypes used, Columbia-0 in our case and Landsberg for *mee57*. If the latter is true, *MET3* function
273 could vary between different *Arabidopsis* accessions.

274 In this work, we show that repression of *MET3* expression at later stages of endosperm
275 development is linked to the direct action of the FIS-PcG complex on the *MET3* locus. *MET3* is over-
276 expressed in PcG mutant seeds, such as *fie* and *msi1* mutant seeds. Interestingly, it was previously

277 shown that *fie* mutant endosperm display higher CG methylation compared to wild-type endosperm
278 and lower CHG and CHH (Ibarra et al. 2012). This increased CG methylation in *fie* mutant seems to be
279 restricted to the endosperm as it is not observed in *fie* seedling or *fie* embryo methylome (Bouyer et
280 al. 2017). We propose that higher expression of *MET3* in the *fie* endosperm could be the cause for the
281 increase in CG methylation specifically in the endosperm. Indeed, in our study, we could not observe
282 any change in *MET3* tissue expression pattern in PcG mutants but the increased expression is still
283 restricted to the endosperm. In further studies, the Investigation of the endosperm methylome in
284 *met3* and *met3;fie* mutants will allow to test this hypothesis. Additionally, further experiments are
285 required to determine if MET3 is a functional DNA methyltransferase.

286 As we previously mentioned, *MET3* function could vary in between wild *Arabidopsis* accessions.
287 Similarly, to CMT1, several SNPs can be found at the *MET3* locus in-between different ecotypes
288 suggesting that *MET3* might not be fully functional in all of them. Additionally, looking closer at the
289 *MET3* locus, we could detect the presence of a Class 2 DNA transposon (*AT4TE34810*) situated in the
290 third intron of the *MET3* gene. In addition to PcG regulation, *MET3* expression and possibly function
291 could be influenced by the presence or regulation of *AT4TE34810* like it is the case for *CMT1* transcript
292 (Yadav et al. 2018). The study of *MET3* function and imprint in different accession could reveal more
293 about its function in natural growth conditions. One hint of *MET3* potential function in Columbia-0
294 came from the study of methylome stability across several generations (Becker et al. 2011). In this
295 study, methylome stability was investigated in several Col-0 selfed lineages (30 generations). The line
296 accumulating the most methylation polymorphisms had concomitantly acquired a SNP in the *MET3*
297 gene. It was therefore suggested that *MET3* could be the cause of such methylome instability (Becker
298 et al. 2011; Schmitz and Ecker 2012). Analyzing the methylome of selfed *met3* mutants after 30
299 generations would allow to test this hypothesis. If true and taking into account the endosperm
300 specificity of *MET3* expression, it would indicate that the endosperm methylome influences the
301 embryonic methylome, a hypothesis that has stimulated a lot of interest over the last 10 years but
302 remains to be demonstrated.

Acknowledgments

We would like to thank the following people for their help: Jasmine Sekulovski for support concerning plant growth, Diane Bonnet for technical support. We thank Mathieu Ingouff and Diane Bonnet for critical reading of the manuscript.

Funding

PEJ and LT are supported by an SNF professorship grant (no.163946) attributed to PEJ.

Author contributions

PEJ conceived the study. LT performed the experiments. LT and PEJ analyzed the data. PEJ wrote the manuscript with the help of LT.

Conflicts of interest

Authors state that there is no conflict of interest.

315 *References*

316 Afgan E, Baker D, Batut B, et al (2018) The Galaxy platform for accessible, reproducible and
317 collaborative biomedical analyses: 2018 update. Nucleic Acids Res 46:W537–W544.
318 https://doi.org/10.1093/nar/gky379

319 Andrews S (2010) FastQC: a quality control tool for high throughput sequence data.

320 Batista RA, Köhler C (2020) Genomic imprinting in plants-revisiting existing models. Genes Dev
321 34:24–36. https://doi.org/10.1101/gad.332924.119

322 Becker C, Hagmann J, Müller J, et al (2011) Spontaneous epigenetic variation in the Arabidopsis
323 thaliana methylome. Nature 480:245–9. https://doi.org/10.1038/nature10555

324 Belmonte MF, Kirkbride RC, Stone SL, et al (2013) Comprehensive developmental profiles of gene
325 activity in regions and subregions of the Arabidopsis seed. Proc Natl Acad Sci 110:E435–E444.
326 https://doi.org/10.1073/pnas.1222061110

327 Berger F (2003) Endosperm: The crossroad of seed development. Curr Opin Plant Biol 6:42–50.
328 https://doi.org/10.1016/S1369526602000043

329 Boisnard-Lorig C, Colon-Carmona A, Bauch M, et al (2001) Dynamic analyses of the expression of the
330 HISTONE::YFP fusion protein in arabidopsis show that syncytial endosperm is divided in mitotic
331 domains. Plant Cell 13:495–509

332 Bolger AM, Lohse M, Usadel B (2014) Trimmomatic: A flexible trimmer for Illumina sequence data.
333 Bioinformatics 30:2114–2120. https://doi.org/10.1093/bioinformatics/btu170

334 Bouyer D, Kramdi A, Kassam M, et al (2017) DNA methylation dynamics during early plant life.
335 Genome Biol 18:179. https://doi.org/10.1186/s13059-017-1313-0

336 Bouyer D, Roudier F, Heese M, et al (2011) Polycomb repressive complex 2 controls the embryo-to-

seedling phase transition. PLoS Genet 7:. https://doi.org/10.1371/journal.pgen.1002014

Brown RC, Lemmon BE, Nguyen H (2003) Events during the first four rounds of mitosis establish three developmental domains in the syncytial endosperm of Arabidopsis thaliana. Protoplasma 222:167–74. https://doi.org/10.1007/s00709-003-0010-x

Brown RC, Lemmon BE, Nguyen H, Olsen OA (1999) Development of endosperm in Arabidopsis thaliana. Sex Plant Reprod 12:32–42. https://doi.org/10.1007/s004970050169

Cao X, Jacobsen SE (2002) Locus-specific control of asymmetric and CpNpG methylation by the DRM and CMT3 methyltransferase genes. Proc Natl Acad Sci U S A 99:16491–16498. https://doi.org/10.1073/pnas.162371599

Chaudhury a M, Ming L, Miller C, et al (1997) Fertilization-independent seed development in Arabidopsis thaliana. Proc Natl Acad Sci U S A 94:4223–8

Chèneby J, Ménétrier Z, Mestdagh M, et al (2020) ReMap 2020: A database of regulatory regions from an integrative analysis of Human and Arabidopsis DNA-binding sequencing experiments. Nucleic Acids Res 48:D180–D188. https://doi.org/10.1093/nar/gkz945

Choi Y, Gehring M, Johnson L, et al (2002) DEMETER, a DNA glycosylase domain protein, is required for endosperm gene imprinting and seed viability in arabidopsis. Cell 110:33–42

Clough SJ, Bent AF (1998) Floral dip: A simplified method for Agrobacterium-mediated transformation of *Arabidopsis thaliana*. Plant J 16:735–743. https://doi.org/10.1046/j.1365-313X.1998.00343.x

Costa LM, Gutièrrez-Marcos JF, Dickinson HG (2004) More than a yolk: The short life and complex times of the plant endosperm. Trends Plant Sci 9:507–514. https://doi.org/10.1016/j.tplants.2004.08.007

359 Gehring M (2013) Genomic imprinting: insights from plants. Annu Rev Genet 47:187–208.
360 https://doi.org/10.1146/annurev-genet-110711-155527

361 Gehring M, Bubb KL, Henikoff S (2009) Extensive demethylation of repetitive elements during seed
362 development underlies gene imprinting. Science (80-) 324:1447–51.
363 https://doi.org/10.1126/science.1171609

364 Gehring M, Huh JH, Hsieh TF, et al (2006) DEMETER DNA Glycosylase Establishes MEDEA Polycomb
365 Gene Self-Imprinting by Allele-Specific Demethylation. Cell 124:495–506.
366 https://doi.org/10.1016/j.cell.2005.12.034

367 Guitton A, Page DR, Chambrier P, et al (2004) Identification of new members of Fertilisation
368 Independent Seed Polycomb Group pathway involved in the control of seed development in
369 Arabidopsis thaliana. Development 2971–2981. https://doi.org/10.1242/dev.01168

370 Henikoff S, Comai L (1998) A DNA Methyltransferase Homolog With a Chromodomain Exists in
371 Multiple Polymorphic Forms in Arabidopsis. Genetics 149:307–318

372 Hsieh TT-F, Ibarra CA, Silva P, et al (2009) Genome-wide demethylation of Arabidopsis endosperm.
373 Science (80-) 324:1451–1454. https://doi.org/10.1126/science.1172417

374 Ibarra CA, Feng X, Schoft VK, et al (2012) Active DNA Demethylation in Plant Companion Cells
375 Reinforces Transposon Methylation in Gametes. Science (80-) 337:1360–1364.
376 https://doi.org/10.1126/science.1224839

377 Jullien PE, Berger F (2009) Gamete-specific epigenetic mechanisms shape genomic imprinting. Curr
378 Opin Plant Biol 12:637–642. https://doi.org/10.1016/j.pbi.2009.07.004

379 Jullien PE, Kinoshita T, Ohad N, Berger F (2006) Maintenance of DNA Methylation during the
380 Arabidopsis Life Cycle Is Essential for Parental Imprinting. Plant Cell 18:1360–1372.

381 https://doi.org/10.1105/tpc.106.041178.1

382 Jullien PE, Susaki D, Yelagandula R, et al (2012) DNA methylation dynamics during sexual
383 reproduction in Arabidopsis thaliana. Curr Biol 22:1825–1830.
384 https://doi.org/10.1016/j.cub.2012.07.061

385 Kim D, Langmead B, Salzberg SL (2015) HISAT: A fast spliced aligner with low memory requirements.
386 Nat Methods 12:357–360. https://doi.org/10.1038/nmeth.3317

387 Kinoshita T, Miura A, Choi Y, et al (2004) One-Way Control of FWA Imprinting in Arabidopsis
388 Endosperm by DNA Methylation. Science (80-) 303:521–523.
389 https://doi.org/10.1126/science.1089835

390 Kinoshita T, Yadegari R, Harada JJ, et al (1999) Imprinting of the MEDEA polycomb gene in the
391 Arabidopsis endosperm. Plant Cell 11:1945–52

392 Kiyosue T, Ohad N, Yadegari R, et al (1999) Control of fertilization-independent endosperm
393 development by the MEDEA polycomb gene in Arabidopsis. Proc Natl Acad Sci 96:4186–4191.
394 https://doi.org/10.1073/pnas.96.7.4186

395 Klepikova A V., Kasianov AS, Gerasimov ES, et al (2016) A high resolution map of the Arabidopsis
396 thaliana developmental transcriptome based on RNA-seq profiling. Plant J 88:1058–1070.
397 https://doi.org/10.1111/tpj.13312

398 Köhler C, Hennig L, Bouveret R, et al (2003) Arabidopsis MSI1 is a component of the MEA/FIE
399 Polycomb group complex and required for seed development. EMBO J 22:4804–14.
400 https://doi.org/10.1093/emboj/cdg444

401 Köhler C, Page DR, Gagliardini V, Grossniklaus U (2005) The Arabidopsis thaliana MEDEA Polycomb
402 group protein controls expression of PHERES1 by parental imprinting. Nat Genet 37:28–30.

https://doi.org/10.1038/ng1495

Liao Y, Smyth GK, Shi W (2014) FeatureCounts: An efficient general purpose program for assigning sequence reads to genomic features. Bioinformatics 30:923–930. https://doi.org/10.1093/bioinformatics/btt656

Lindroth a M, Cao X, Jackson JP, et al (2001) Requirement of CHROMOMETHYLASE3 for maintenance of CpXpG methylation. Science 292:2077–80. https://doi.org/10.1126/science.1059745

Liu J, Deng S, Wang H, et al (2016) CURLY LEAF regulates gene sets coordinating seed size and lipid biosynthesis. Plant Physiol 171:424–436. https://doi.org/10.1104/pp.15.01335

Love MI, Huber W, Anders S (2014) Moderated estimation of fold change and dispersion for RNA-Seq data with DESeq2. bioRxiv 1–21. https://doi.org/10.1101/002832

Luo M, Bilodeau P, Dennis ES, et al (2000) Expression and parent-of-origin effects for FIS2, MEA, and FIE in the endosperm and embryo of developing Arabidopsisseeds. PNAS. https://doi.org/10.1073/pnas.170292997

Luo M, Bilodeau P, Koltunow a, et al (1999) Genes controlling fertilization-independent seed development in Arabidopsis thaliana. Proc Natl Acad Sci U S A 96:296–301

Mi H, Muruganujan A, Huang X, et al (2019) Protocol Update for large-scale genome and gene function analysis with the PANTHER classification system (v.14.0). Nat Protoc 14:703–721. https://doi.org/10.1038/s41596-019-0128-8

Ohad N, Yadegari R, Margossian L, et al (1999) Mutations in FIE, a WD polycomb group gene, allow endosperm development without fertilization. Plant Cell 11:407–415. https://doi.org/10.1105/tpc.11.3.407

Pagnussat GC, Yu HJ, Ngo QA, et al (2005) Genetic and molecular identification of genes required for

425 female gametophyte development and function in Arabidopsis. Development 132:603–614.
426 https://doi.org/10.1242/dev.01595

427 Quadrana L, Silveira AB, Mayhew GF, et al (2016) The Arabidopsis thaliana mobilome and its impact
428 at the species level. Elife 5:1–25. https://doi.org/10.7554/eLife.15716

429 Salvador-Guirao R, Baldrich P, Weigel D, et al (2018) The MicroRNA miR773 Is Involved in the
430 *Arabidopsis* Immune Response to Fungal Pathogens. Mol Plant-Microbe Interact 31:249–259.
431 https://doi.org/10.1094/MPMI-05-17-0108-R

432 Schmitz RJ, Ecker JR (2012) Epigenetic and epigenomic variation in Arabidopsis thaliana. Trends Plant
433 Sci 17:149–154. https://doi.org/10.1016/j.tplants.2012.01.001

434 Sørensen MB, Chaudhury AM, Robert H, et al (2001) Polycomb group genes control pattern
435 formation in plant seed. Curr Biol 11:277–281

436 Stroud H, Do T, Du J, et al (2013) Non-CG methylation patterns shape the epigenetic landscape in
437 Arabidopsis. Nat Struct Mol Biol 21:64–72. https://doi.org/10.1038/nsmb.2735

438 Supek F, Bošnjak M, Škunca N, Šmuc T (2011) Revigo summarizes and visualizes long lists of gene
439 ontology terms. PLoS One 6:. https://doi.org/10.1371/journal.pone.0021800

440 Weinhofer I, Hehenberger E, Roszak P, et al (2010) H3K27me3 Profiling of the Endosperm Implies
441 Exclusion of Polycomb Group Protein Targeting by DNA Methylation. PLoS Genet 6:e1001152.
442 https://doi.org/10.1371/journal.pgen.1001152

443 Winter D, Vinegar B, Nahal H, et al (2007) An “electronic fluorescent pictograph” Browser for
444 exploring and analyzing large-scale biological data sets. PLoS One 2:1–12.
445 https://doi.org/10.1371/journal.pone.0000718

446 Yadav NS, Khadka J, Domb K, et al (2018) CMT3 and SUVH4/KYP silence the exonic Evelknievel

447 retroelement to allow for reconstitution of CMT1 mRNA 06 Biological Sciences 0604 Genetics.
448 Epigenetics and Chromatin 11:1–12. https://doi.org/10.1186/s13072-018-0240-y

449 Yadegari R, Kinoshita T, Lotan O, et al (2000) Mutations in the FIE and MEA genes that encode
450 interacting polycomb proteins cause parent-of-origin effects on seed development by distinct
451 mechanisms. Plant Cell 12:2367–2382

452 Zhang X, Clarenz O, Cokus S, et al (2007) Whole-genome analysis of histone H3 lysine 27
453 trimethylation in Arabidopsis. PLoS Biol 5:e129. https://doi.org/10.1371/journal.pbio.0050129

454

455

456 *Figure legends*

457 *Figure 1. MET3 expression pattern*

458 (a) *MET3* expression measured by RT-qPCR. DAP = Day After Pollination. The histogram displays the
459 mean, and each dot represents a biological replicate. *ACT2* is used as a normalizer. RQ = Relative
460 Quantification (b-e) Single-plan Confocal images representing the expression of *pMET3:H2B-*
461 *tdTomato* construct in *Arabidopsis* 1 Day After Synchronization (DAS) seed (b), 2 DAS seed (c), 3 DAS
462 (d) and 5 DAS (e). cze = chalazal endosperm, endo = endosperm nuclei. Scale bars represent 25µm.

463 *Figure 2. MET3 is biallelically expressed with a paternal bias*

464 (a) Allele specific RT-PCR of *MET3* parental expression in 5DAP silique samples. The *XbaI* restriction
465 enzyme digests the Col-0 *MET3* transcript but not the Gr-1 transcript. *ACT2* is used as loading control.
466 (b) Single-plan confocal images of *pMET3:H2B-RFP* parental expression in the endosperm of 1 DAP
467 seeds. endo = endosperm nuclei. Scale bars represent 25µm. ♂ symbol indicates the genotype of the
468 male parent while ♀ indicates the genotype of the female parent.

469 *Figure 3. MET3 expression is controlled by FIE and MSI1 Polycomb proteins*

470 (a-c) Confocal images representing the expression of *pMET3:H2B-RFP* construct in *Arabidopsis*
471 wildtype (a), *fie* (b) and *msi1* (c) selfed seeds at 5 days after pollination (DAP). Scale bars represent 50
472 µm. (d) Proportion of seeds with high RFP signal in the endosperm at 5DAP in wild-type, *fie* and *msi1*
473 mutants. Grey bars represent the seeds with a restricted RFP expression to the chalazal endosperm
474 (as illustrated in (a)). Black bars represent the seeds with ectopic expression of *pMET3:H2B-RFP*
475 throughout the endosperm (as illustrated in (b-c)). (e) *MET3* expression measured by RT-qPCR in 10
476 DAP selected seeds of wild-type, *fie* and *msi1*. The histogram displays the mean, and each dot
477 represents a biological replicate. *ACT2* is used as a normalizer. (f) Snapshot showing that the *MET3*
478 locus contains H3K27me3 and LHP1 but no H3K4me1, H3K4me2, H3K4me3 and H3K9me2 in seedlings.
479 Data from http://epigenomics.mcdb.ucla.edu/H3K27m3/ (Zhang et al. 2007).

480 *Figure 4. MET3 does not influence fie phenotype*

481 (a-f) Seed developmental phenotype observed after clearing by Difference Interference Contrast (DIC)
482 of wild-type (a), *met3-3* (b), *met3-4* (c), *fie/+* (d), *met3-3;fie/+* (e) and *met3-4;fie/+* (f) at 6 days after
483 synchronization (DAS). Scale bars represent 50 µm. (g-h) Quantification of the embryo developmental
484 stages (g) and endosperm cellularization (h) in wild-type, *met3-3*, *met3-4*, *fie/+*, *met3-3;fie/+* and
485 *met3-4;fie/+* at 6 DAS. mce = micropylar endosperm.

486 *Figure 5. Transcriptome of met3 and met3;fie mutant seeds*

487 (a-b) Volcano plot depicting differentially expressed genes (DEGs) comparing Col-0 to *met3-3* (a) and
488 *fie* to *met3-3;fie* in 10 DAS seeds (b). Red dots represent up-regulated DEGs and blue dots represent
489 down-regulated DEGs. The top 10 DEGs are annotated. We use a threshold of [absolute logFC > 2,
490 FDR < 0.05]. (c) GO term analysis for the 87 DEGs obtained with the *fie vs met3-3;fie* contrast. (d)
491 Venn diagram showing the overlapping DEGs between the different contrasts.

492 *Figure S1. MET3 is only expressed in seeds*

493 (a) Snapshot of the *MET3* expression pattern obtained from ebar using the data from Klepikova *et al.*
494 (Winter et al. 2007; Klepikova et al. 2016)(b-d) The absence of *pMET3:H2B-GUS* expression observed
495 in *Arabidopsis* seedling (b), stamen (c) and ovule (d).

496 *Figure S2. MET3 reporters and expression*

497 (a) Representation of *pMET3:H2B-GUS*, *pMET3:H2B-tdTomato* and *pMET3:H2B-RFP*. (b) *pMET3:H2B-*
498 *GUS* expression observed in 1 DAP and 3 DAP seeds. (c) *pMET3:H2B-RFP* expression observed in 1 DAP
499 and 3 DAP seeds. Scale bars represent 50 µm. (d) Snapshot of expression data from LCM dissected
500 seeds from http://seedgenenetwork.net/plotprobe?name=254720_at (Belmonte et al. 2013).

501 *Figure S3. MET3 regulation by Polycomb group*

502 (a) *MET3* expression from an RNA-seq experiment in inflorescence, root, shoot and siliques from wild-
503 type plants and *clf28* mutant plants, data from Liu *et al* 2016 (Liu et al. 2016). (b) *MET3* expression

504 from transcriptomic data obtained from 3 DAP seeds using MicroArray comparing wild-type to *fis2-1*
505 endosperm, data from Weinhofer *et al* 2010 (Weinhofer et al. 2010). (c) Snapshot of H3K27me3 ChIP
506 data from several tissues including endosperm (colored in blue), flowers (colored in yellow) and
507 various sporophytic (colored in green). Green line represent the presence of ChIP peaks of H3K27me3.
508 Data from ReMap (Chèneby et al. 2020).

509 *Figure S4. Characterization of MET3 mutants*

510 (a) Representation of the *MET3* locus. Blue triangles are representing the T-DNA insertion site of both
511 *met3-3* (GABI_404F04) and *met3-4* (GABI_659H03) (b) *MET3* expression measured by RT-qPCR in Col-
512 0 and *met3* mutants seeds at 3DAP. The histogram displays the mean, and each dot represents a
513 biological replicate. *ACT2* is used as a normalizer. 2 stars indicate a p value <0.01.

514 *Figure S5. MET3 mutants do not show developmental defect*

515 (a) Percentage of seed abortion in Col-0 and *met3* mutants (*met3-3* and *met3-4*) siliques. (b) met3
516 mutants transmission in self progeny. +/+ represent wild-type, +/- heterozygotes and -/- homozygotes
517 plants for the mutation. (c) Seed size measurement for Col-0 and *met3* mutants dry seeds. No
518 significant differences observed. (d) Pictures of Col-0 and *met3* mutants dry seeds. The scale bars
519 represent 1 mm.

520 *Figure S6. Transcriptome of met3 mutant seeds at 3DAP*

521 (a-b) Volcano plot depicting one differentially expressed gene comparing Col-0 to *met3-3* (a) and
522 *met3-4 (b)* at 3DAP.

523

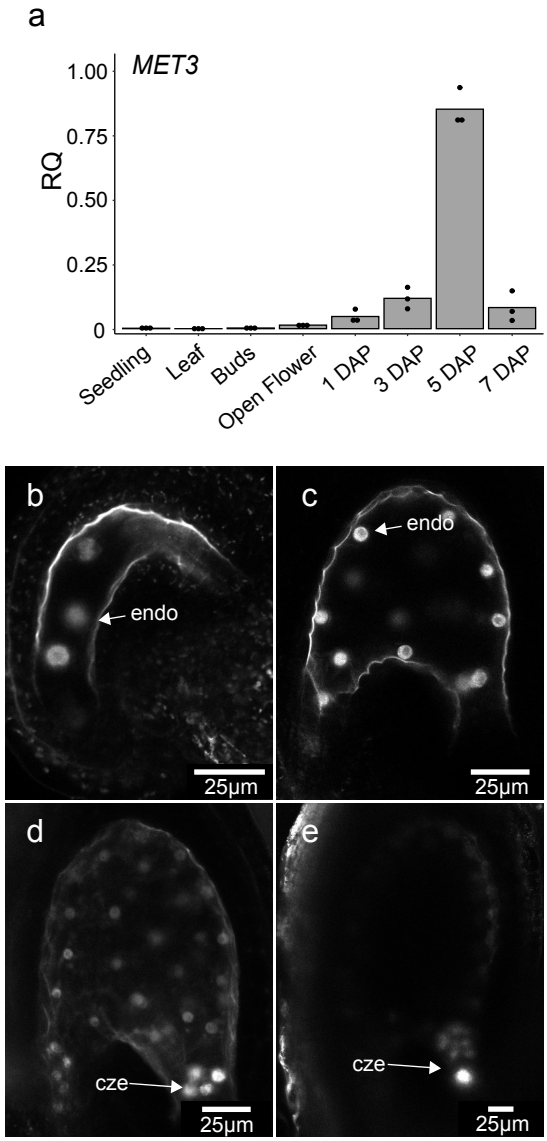

Figure 1. *MET3* expression pattern

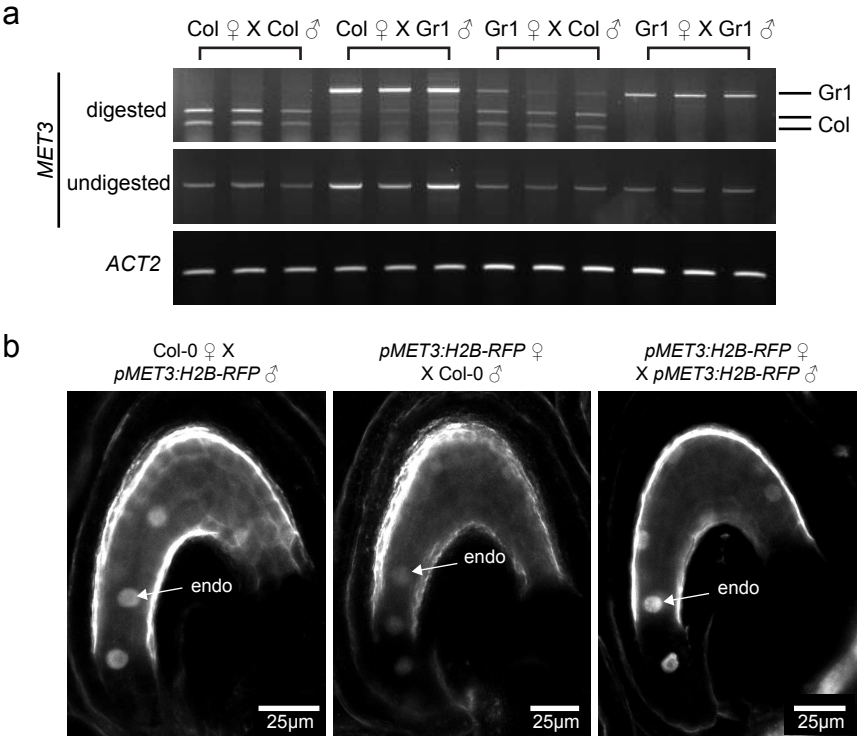

Figure 2. *MET3* is biallelically expressed with a paternal bias

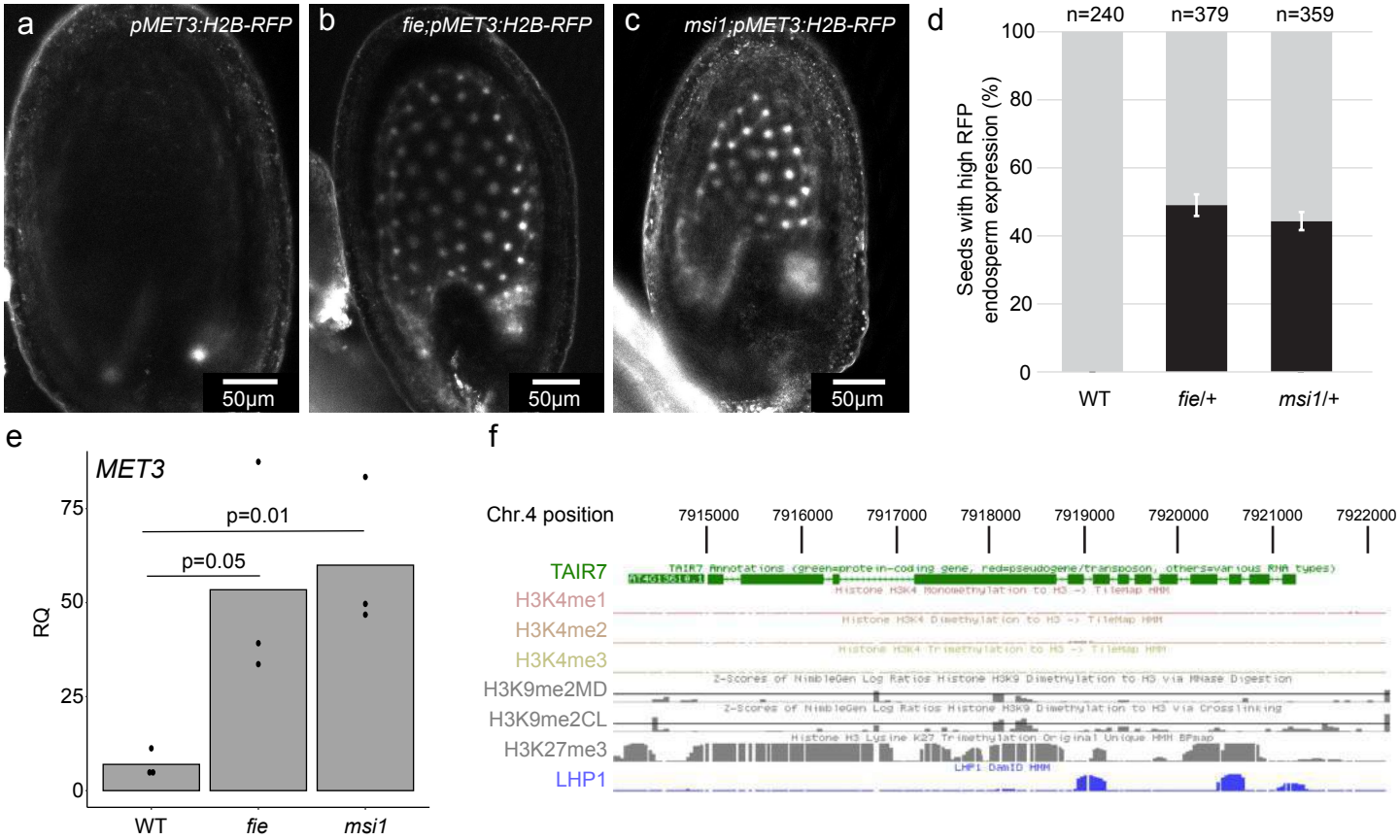

Figure 3. *MET3* expression is controlled by *FIE* and *MSI1* Polycomb proteins

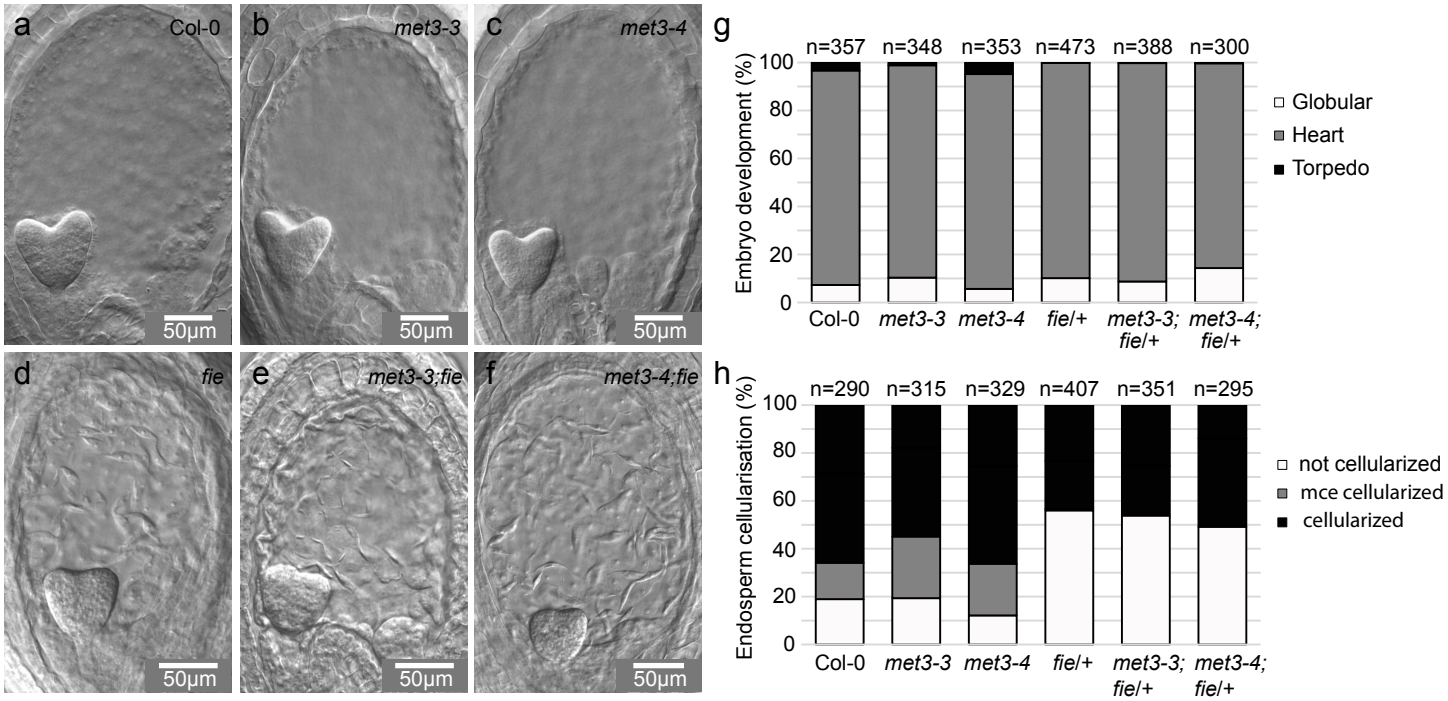

Figure 4. *MET3* does not influence *fie* phenotype

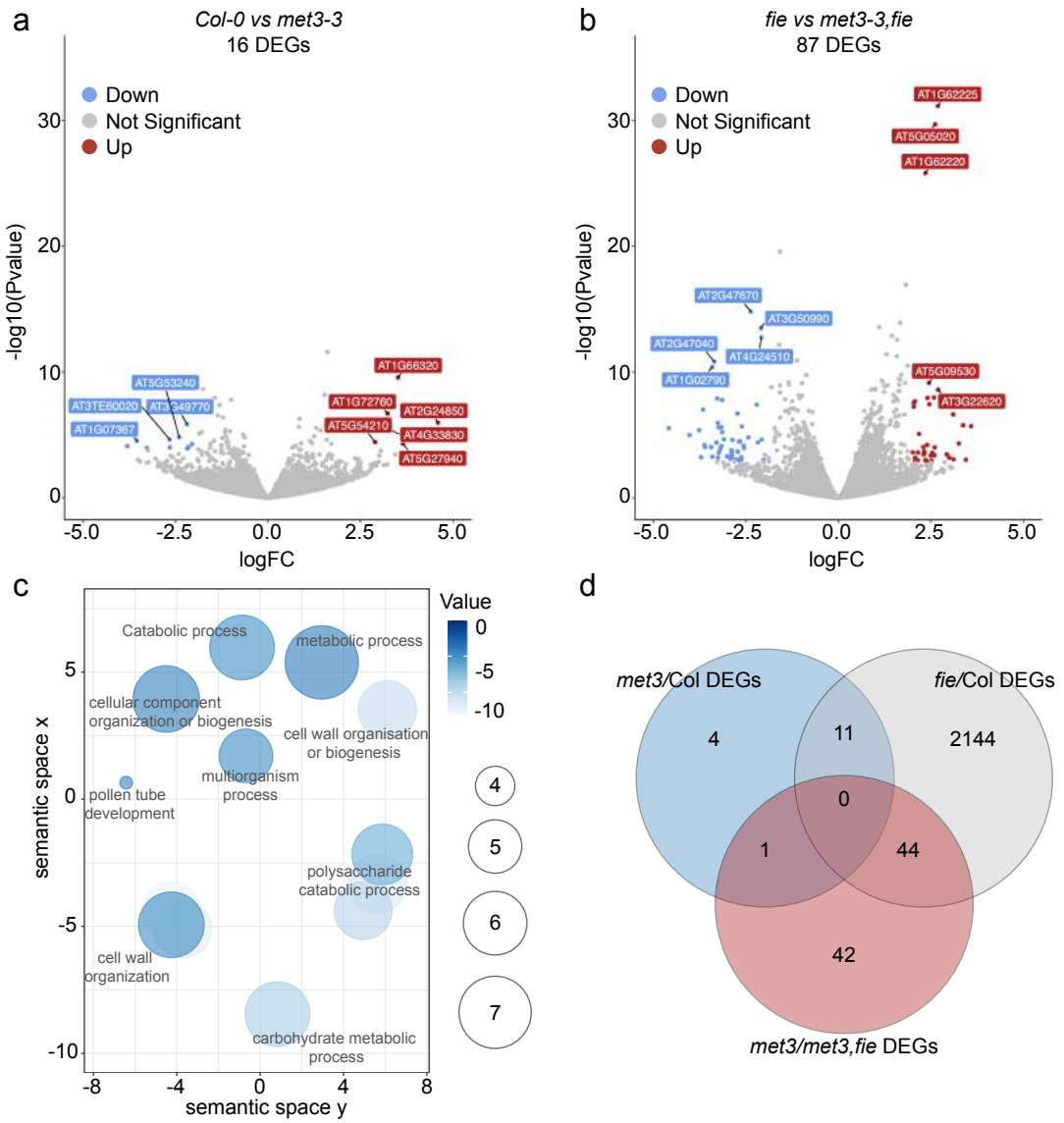

Figure 5. Transcriptome of *met3* and *met3fie* mutant seeds

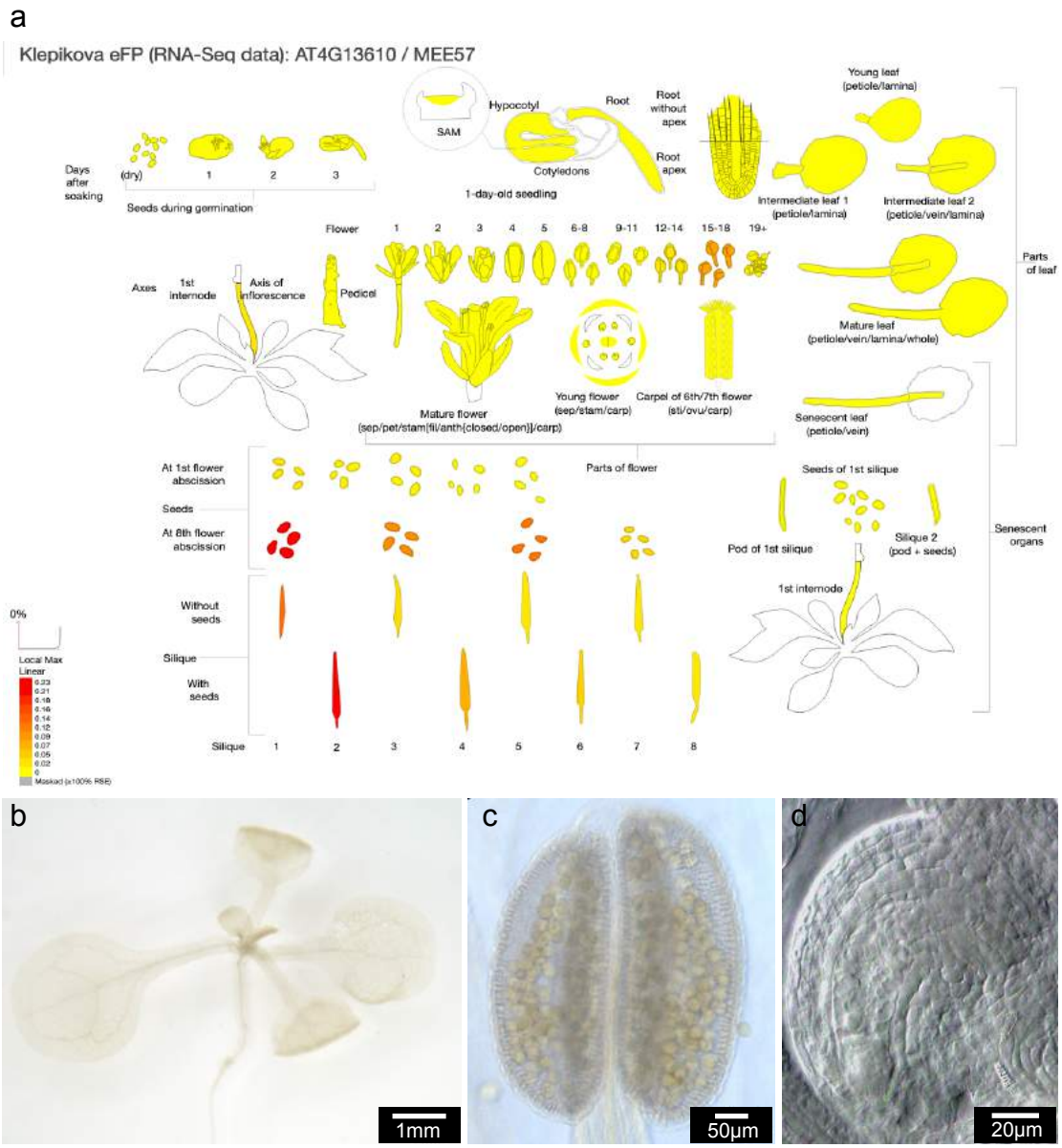

Figure S1. *MET3* is only expressed in seeds

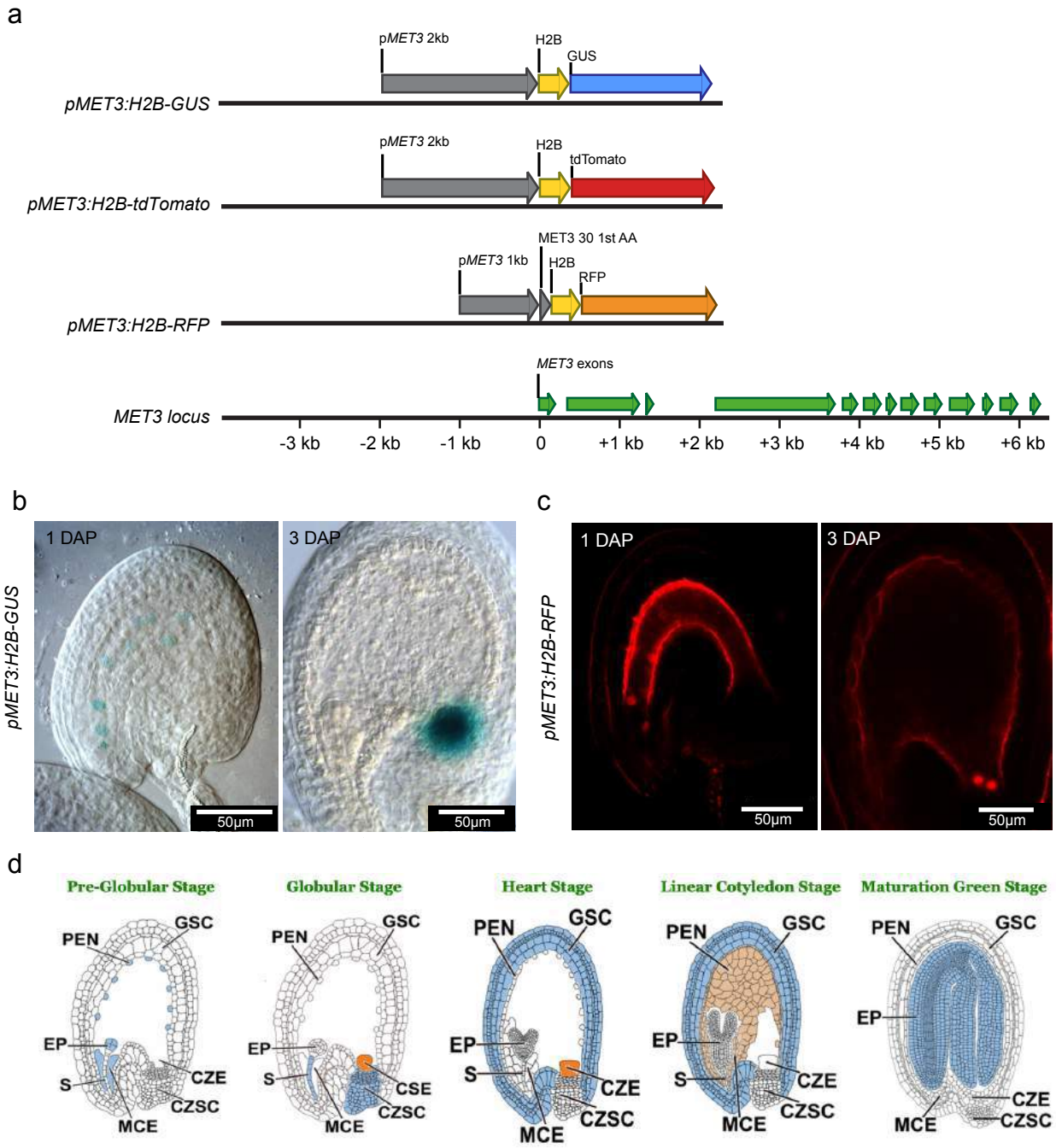

Figure S2. *MET3* reporters and expression

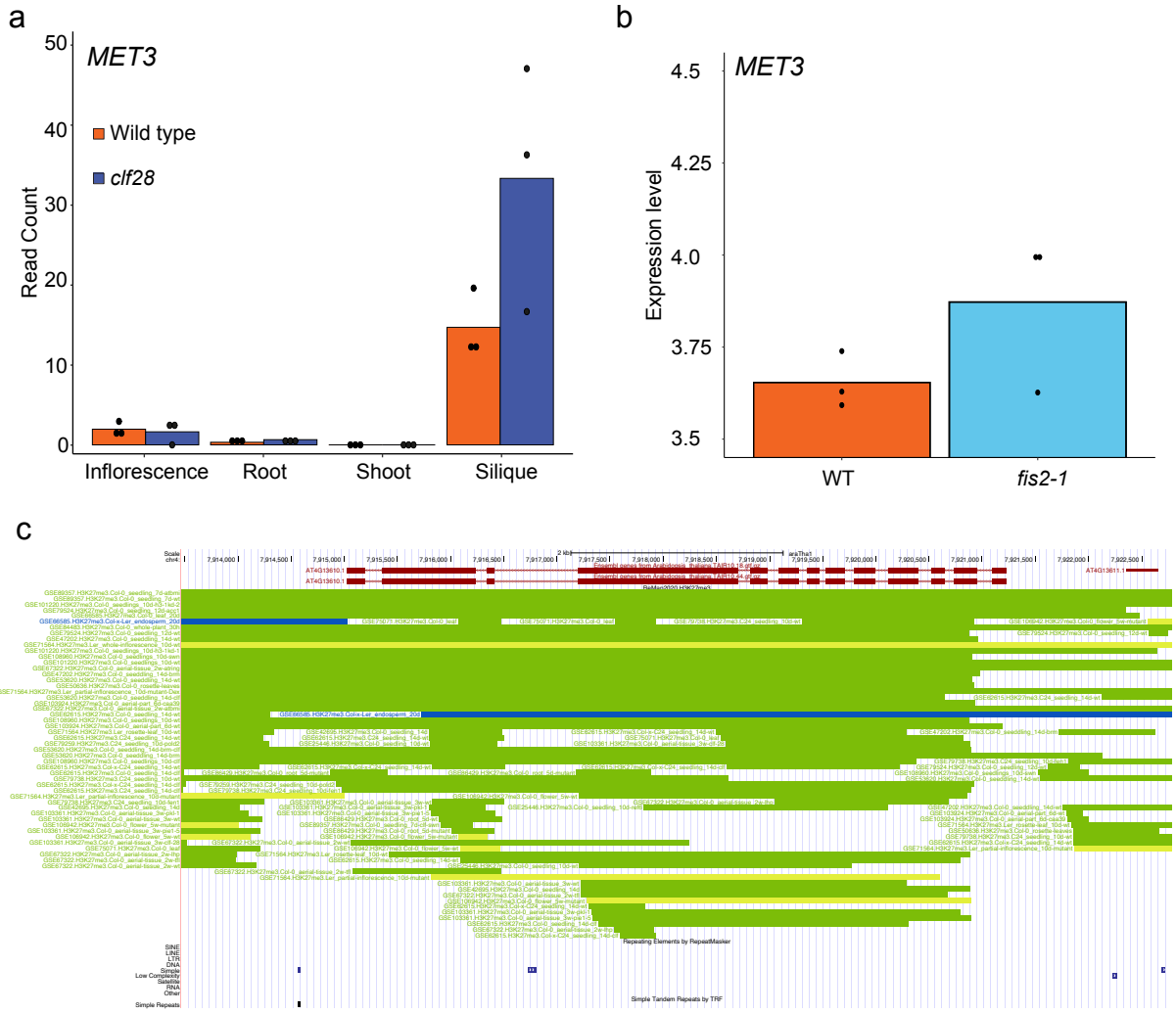

Figure S3. *MET3* regulation by Polycomb group

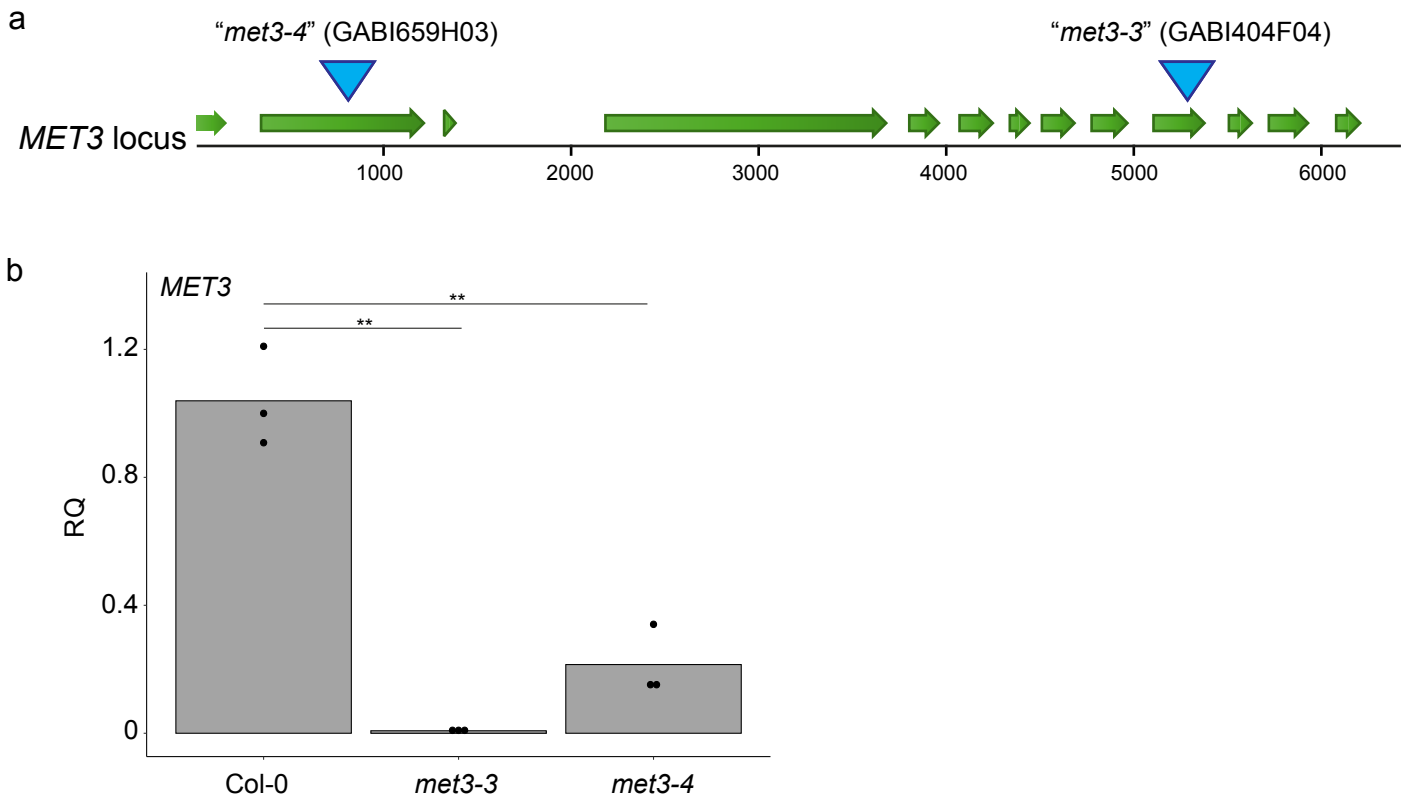

Figure S4. Characterization of *MET3* mutants

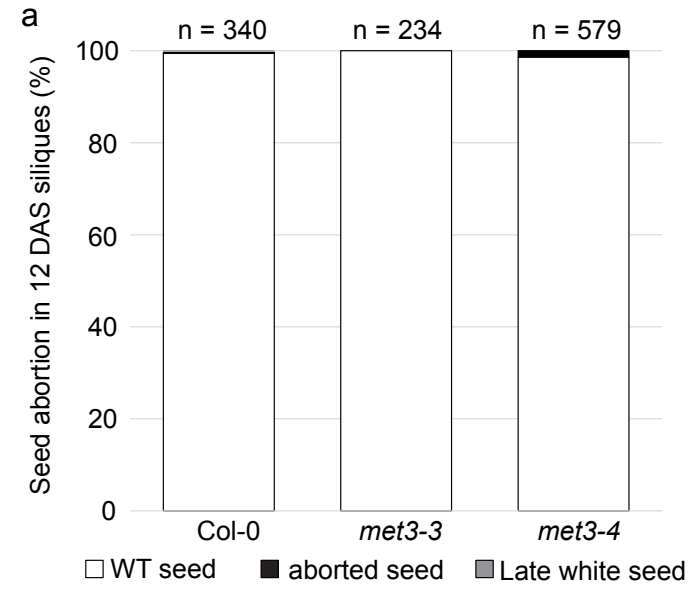

b

genotype	*met3-3/+*	*met3-4/+*
+/+	44 (25%)	39 (23.07%)
-/+	97 (55.11%)	85 (50.09%)
-/-	35 (19.88%)	45 (26.62%)
Total	176 (100%)	169 (100%)
χ2 test	p=0.251	p=0.806

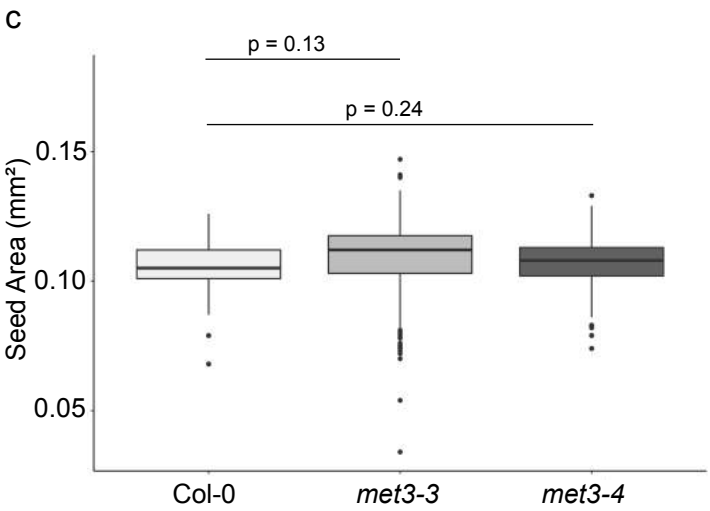

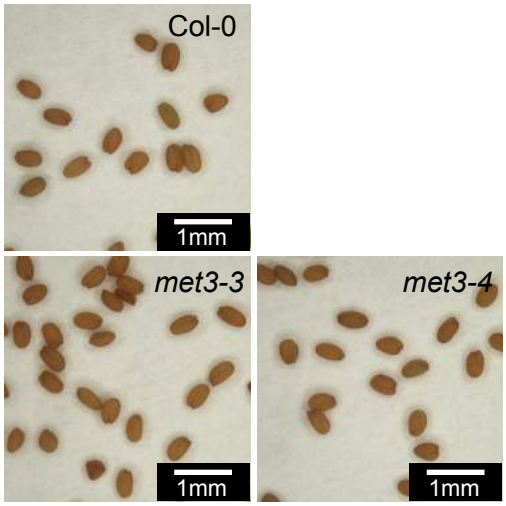

Figure S5. *MET3* mutant do not show developmental defect

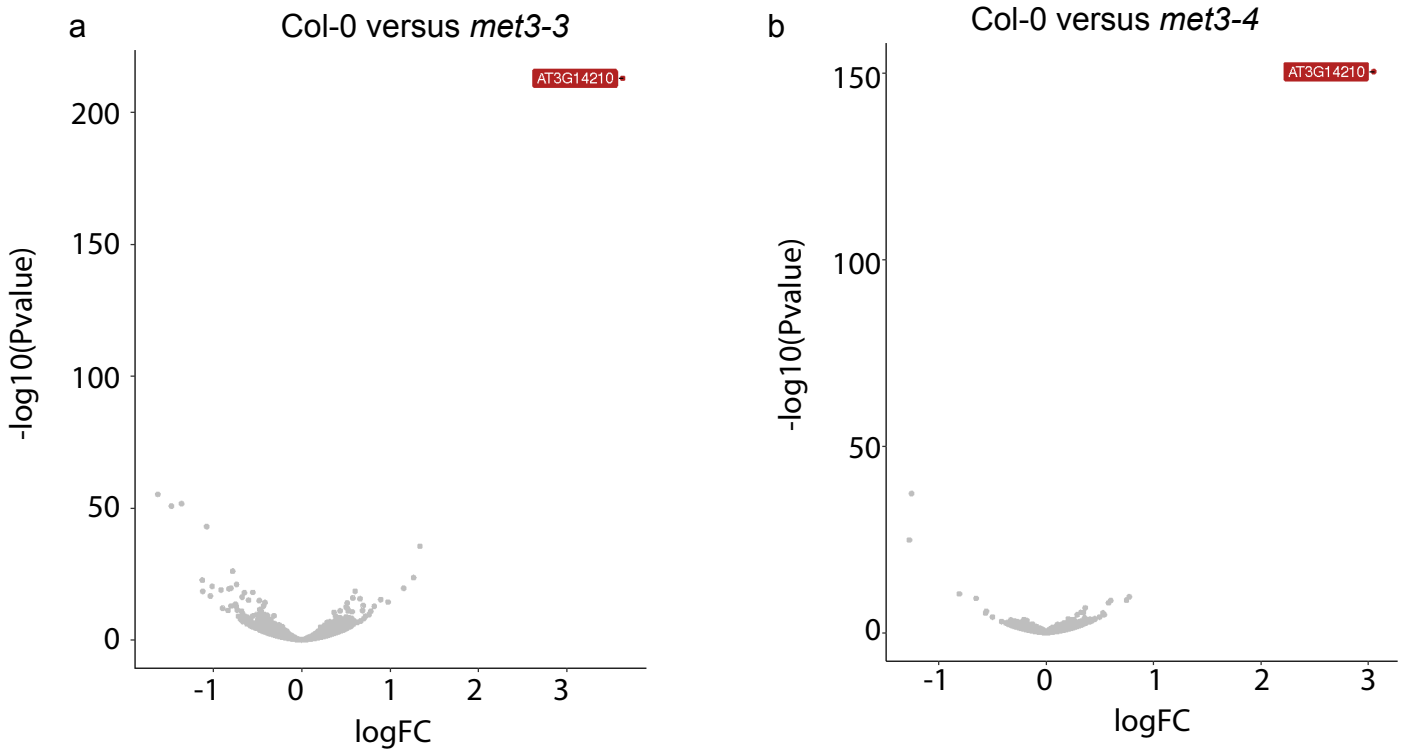

Figure S6. Transcriptome of *met3* mutant seeds at 3DAP